



# Damage threshold of LiF crystal irradiated by femtosecond hard XFEL pulse sequence

SERGEY MAKAROV,<sup>1,\*</sup> SERGEY GRIGORYEV,<sup>1</sup> NAIL INOGAMOV,<sup>2,1</sup> EVGENY FILIPPOV,<sup>1</sup> TATIANA PIKUZ,<sup>3</sup> NORIMASA OZAKI,<sup>4,5</sup> MASAHICO ISHINO,<sup>6</sup> MASAHARU NISHIKINO,<sup>6</sup> THANH-HUNG DINH,<sup>6</sup> TETSUYA KAWACHI,<sup>6</sup> MAXIM ZANAVESKIN,<sup>7</sup> MIKAKO MAKITA,<sup>8</sup> MOTOAKI NAKATSUTSUMI,<sup>8</sup> THOMAS R. PRESTON,<sup>8</sup> KAREN APPEL,<sup>8</sup> ZUZANA KONOPKOVA,<sup>8</sup> VALERIO CERANTOLA,<sup>8</sup> ERIK BRAMBRINK,<sup>8</sup> JAN-PATRICK SCHWINKENDORF,<sup>8</sup> ISTVÁN MOHACSI,<sup>8</sup> VOJTECH VOZDA,<sup>9</sup> VERA HAJKOVA,<sup>9</sup> TOMAS BURIAN,<sup>9</sup> JAROMIR CHALUPSKY,<sup>9</sup> LIBOR JUHA,<sup>9</sup> VASILY ZHAKHOVSKY,<sup>1</sup> ULF ZASTRAU,<sup>8</sup> AND SERGEY PIKUZ<sup>1</sup>

<sup>1</sup>Joint Institute for High Temperatures Russian Academy of Sciences, Moscow 125412, Russia

<sup>2</sup>Landau Institute for Theoretical Physics, Russian Academy of Sciences, Chernogolovka, Moscow Region, 142432, Russia

<sup>3</sup>Institute for Open and Transdisciplinary Research Initiatives, Osaka University, 2-6 Yamadaoka, Suita, Osaka 565-0871, Japan

<sup>4</sup>Graduate School of Engineering, Osaka University, 2-1 Yamadaoka, Suita, Osaka 565-0871, Japan

<sup>5</sup>Photon Pioneers Center, Osaka University, Suita, Osaka 565-0871, Japan

<sup>6</sup>Kansai Photon Science Institute, National Institutes for Quantum Science and Technology, 8-1-7 Umemidai, Kizugawa, Kyoto 619-0215, Japan

<sup>7</sup>National Research Centre “Kurchatov Institute,” Moscow, 123182, Russia

<sup>8</sup>European XFEL, GmbH, 22869 Schenefeld, Germany

<sup>9</sup>Department of Radiation and Chemical Physics, Institute of Physics, Czech Academy of Sciences, Na Slovance 2, 182 00 Prague 8, Czech Republic

\*seomakarov28@gmail.com

**Abstract:** Here we demonstrate the results of investigating the damage threshold of a LiF crystal after irradiating it with a sequence of coherent femtosecond pulses using the European X-ray Free Electron Laser (EuXFEL). The laser fluxes on the crystal surface varied in the range  $\sim 0.015\text{--}13\text{ kJ/cm}^2$  per pulse when irradiated with a sequence of 1-100 pulses ( $t_{\text{pulse}} \sim 20\text{ fs}$ ,  $E_{\text{ph}} = 9\text{ keV}$ ). Analysis of the surface of the irradiated crystal using different reading systems allowed the damage areas and the topology of the craters formed to be accurately determined. It was found that the ablation threshold decreases with increasing number of X-ray pulses, while the depth of the formed craters increases non-linearly and reaches several hundred nanometers. The obtained results have been compared with data already available in the literature for nano- and picosecond pulses from lasers in the soft X-ray/VUV and optical ranges. A failure model of lithium fluoride is developed and verified with simulation of material damage under single-pulse irradiation. The obtained damage threshold is in reasonably good agreement with the experimentally measured one.

© 2023 Optica Publishing Group under the terms of the [Optica Open Access Publishing Agreement](#)

## 1. Introduction

Exposure of dielectrics to high energy fluxes of ultrashort laser pulses can lead to the damage of the material. The investigation of such interaction and the determination of the threshold at

which the ablation of a substance begins is of interest both from a practical point of view for the development of laser technologies and from a theoretical point of view for the development of models for the strength and destruction of materials.

Nowadays, lasers are widely used in lithography [1,2], the basis for the production of microfluidic chips [3], in the production of volumetric sub-micron structures [4], in the creation of meta-optical devices and in the modification of surface properties by growing nanostructures with a specific topology [5,6], color printing [7] and etc. The important direction in the physics of interaction of laser radiation with matter is associated with lasers with ultrashort pulses. The duration of such pulses ranges from femtoseconds (fs) to picoseconds (ps). The extremely short duration of exposure is associated with a number of advantages over conventional nanosecond and microsecond lasers. In drilling, for example, lateral energy losses are greatly reduced, and the quality of holes and cuts is significantly improved. The mechanisms of surface structure formation change fundamentally. In the case of nanosecond exposure, this is the evaporation of the substance, while the occurrence of amplitude-controlled thermomechanical stresses and the thermomechanical processing of the substance are associated with ultrafast exposure.

The newest direction is associated with the use of ultra-short pulses with a small wavelength in the X-ray range (of the order of 0.1–10 nm) [8]. In X-ray lithography, this enables the production of chips with packing details of units and tens of nanometers. In this case, the transition to photon fluxes with energies of the order of or above the ionization potential of the inner shells of the atoms fundamentally changes the physics of the interaction process and, in considering it, requires the synthesis of approaches developed in solid-state physics with those of plasma physics.

Let us compare the physics of interaction with matter in the case of optical lasers and in the case of the hard X-ray laser considered in this article. This will help us to better understand the specifics of the effect of the hard photon beam. In the optical case, the situation depends on the arrangement of the electronic spectrum, i.e. whether there is a gap in the spectrum or not - therefore there is a qualitative difference between the behavior of metals and dielectrics under optical exposure. We are talking here about the energy gap that separates the conduction band from the filled valence bands in the electronic spectrum. While in metals the absorption of optical radiation is linearly proportional to the intensity of the incident radiation and is localized near the surface in a thin skin layer of the metal, 10-20 nm thick (metal is opaque to optics), the situation with dielectrics is more complicated with the absorption of optical radiation. Such phenomenon as optical breakdown is associated with dielectrics [9,10]. Single or multiphoton ionization and electron avalanches take place [9,10]. As a result of these processes, an electron is excited across the energy gap and the conduction zone is filled up accordingly. In this way, an increasingly dense (as new excitations keep occurring) electron-hole plasma is formed in the dielectric [10]. In the case of hard photons, the main contribution to the absorption is due to the excitation of deep electron shells. The influence of the gap in the electronic spectrum disappears. The gap is related to the outer shells, which have low energy. In this sense, qualitatively, the behavior of metals and dielectrics with respect to absorption of hard radiation is similar. Although, of course, the attenuation length, the role of thermal conductivity may differ significantly depending on the particular dielectric or metal. It is important to note that there is no optical breakdown phenomenon in dielectrics when illuminated by X-rays. Starting at weak fluxes, the absorption of hard X-rays is simply proportional to the intensity of the radiation; here we have drawn away from such a phenomenon as the emptying of inner shells ("hollow" ions) in the field of very intense X-rays [11,12]. In the case of optical irradiation of dielectrics, on the other hand, the absorption increases sharply (i.e., it depends strongly nonlinearly on the intensity) when the concentration of the electron-hole plasma exceeds a critical value. At a critical concentration, the plasma frequency of the electron-hole plasma becomes greater than that of the optical laser.

With the advent of X-ray free-electron lasers, it became possible to study matter under the influence of high energy fluxes that were previously inaccessible. With coherent femtosecond X-ray pulses focused to a size of a few hundred nanometers, volume energy densities of tens and hundreds of MJ/cm<sup>3</sup> can be achieved. It should be noted that for the development of laser technologies, it is necessary to accurately measure the amount of absorbed energy at which material damage/ablation occurs.

Lithium fluoride (LiF) crystal is one of the widely used dielectrics for laser-substance interaction studies. This material is used to make optical windows, prisms and lenses for the ultraviolet (UV), visible and infrared (IR) regions of the spectrum. In addition, the LiF crystal is actively used as a fluorescence detector in X-ray diffraction experiments as an alternative for image plates because it offers submicron spatial resolution and is resistant to high radiation fluxes [13–15]. Due to the latter fact, it can be installed as close as possible to the target in laser plasma experiments (in contrast to CCD matrices) to implement phase-contrast X-ray diffraction and thus reduce the blurring of the final image due to diffraction effects. Knowledge of the destruction threshold of a given dielectric when exposed to high-intensity laser radiation is necessary for the development of various applied fields of physics, as well as for the verification of numerical codes describing such an effect.

The investigation of LiF ablation threshold under nano/picosecond optical lasers and soft X-ray/EUV lasers has been widely reported in the literature [16–21], while there are no data for femtosecond hard pulses of XFELs. In particular, in works [17–19], the threshold value of fluence after which ablation begins and a crater form on the crystal surface was determined for LiF. In particular, the ablation threshold for a LiF crystal was found to be 10 mJ/cm<sup>2</sup> for the wavelength  $\lambda = 13.9$  nm, which is more than two orders of magnitude below the threshold for the case of optical laser irradiation ( $\lambda = 1053$  nm) and below the thresholds in the case of nanosecond pulses of X-ray lasers ( $\lambda = 46.9$  nm). The aim of our work was to extend the knowledge about the interaction of ultra-intense X-ray pulses with the LiF dielectric and to determine the ablation/damage threshold of this material under the influence of hard XFEL femtosecond pulses.

## 2. Experimental procedure

### 2.1. Laser damage of LiF crystal

The experiment was performed at the European X-ray Free Electron Laser (EuXFEL) at the High Energy Density instrument (HED). The scheme of the experiment is shown in Fig. 1. An X-ray beam with a pulse duration of  $\sim 20$  fs and a photon energy of 9 keV ( $\lambda = 0.138$  nm) was focused through beryllium compound refractive lenses (CRLs) into a spot with a size  $\sim 410$  nm at full width at half maximum (FWHM) (for more details on the measurement of the spot size for this experiment, see [22]).

A circle LiF crystal with a diameter of 20 mm and a thickness of 2 mm was irradiated with EuXFEL radiation in modes of 1, 3, 10, 30 and 100 pulses per exposure at a frequency of 10 Hz. The average pulse energy was determined to be 17  $\mu$ J/pulse with the estimated errors of 10%. After each irradiation, the crystal was moved perpendicular to the beam so that the next irradiation fell on a clean sample surface. To find the threshold laser fluence  $F_{th}$  for the onset of LiF damage, the crystal moved at different planes from the theoretical focus along the beam propagation. This approach allowed the value of the laser fluence  $F$  to be varied by increasing the beam size with distance from the focal area. As an example, the upper part of Fig. 1 shows the results of the scanning electron microscope (SEM) measurements after a single pulse irradiation of the crystal. The laser fluence varied in the range of 0.015 – 13 kJ/cm<sup>2</sup> per pulse. The value of the absorbed dose  $D$  (energy deposition per unit volume) can be calculated using the formula  $D = F/d_{att}$ , where  $d_{att}$  is the attenuation length in the material. Considering that the attenuation length in the LiF crystal is  $d_{att} = 475$   $\mu$ m for 9 keV photons [23], the dose

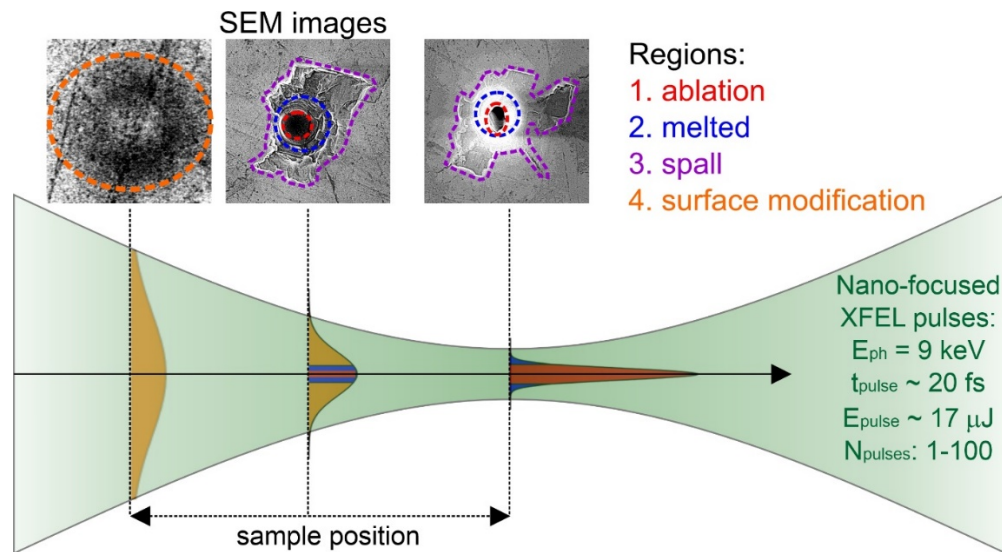


**Fig. 1.** – Scheme of the irradiation of the LiF crystal in this work. The diameter of the cross-section of the XFEL beam (green) is  $\sim 410$  nm in the focal plane. The crystal moves along the focusing axis of the X-ray beam. Above you can see examples of SEM measurements of the surface of an exposed LiF crystal in different planes. The areas with structural changes are marked with different colors.

rate ( $D_{rate}$  is the absorbed dose per pulse) for the different exposures varied in the range of 0.32 – 270 kJ/cm<sup>3</sup>/pulse.

## 2.2. Read-out procedure

To obtain a more complete picture of the consequences of the interaction of X-ray pulses with a LiF crystal, surface of an exposed sample was scanned using several read out systems.

Since the LiF crystal is a fluorescent medium, when it is irradiated with ionizing radiation, color centers (CCs) form in it whose distribution corresponds to the irradiation region. To obtain information about the intensity distribution inside the incident beam, we used a confocal laser scanning microscope CLSM700 from Carl Zeiss. A laser with a pump wavelength of 488 nm allowed excitation of F-type color centers ( $F_2$  and  $F_3^+$ ) whose emission spectrum lies in the optical range (500-800 nm) [24]. The signal was read out from a depth of  $\sim 1$   $\mu$ m using a 100 $\times$  objective with a pixel size of 0.25  $\mu$ m (field of view  $200 \times 200$   $\mu$ m<sup>2</sup>).

To study the damage and modification of the crystal surface, we used an atomic force microscope (AFM) equipped in a scanning laser microscope (OLS4500, Olympus Corp.) and a scanning electron microscope (SEM) (HELIOS NANOLAB 600I, FEI).

It is important to use both the AFM and SEM for our analysis, as both microscopes can provide complementary information. Indeed, the AFM has several advantages over SEM, the most important of which is the ability to obtain a three-dimensional surface profile. In addition, the AFM does not require special surface treatments (such as metal/carbon coatings) that permanently alter or damage the sample. SEM observation enables us to confirm the real structures with a higher spatial resolution than of an optical microscope.

### 3. Experimental results and discussion

#### 3.1. Damage threshold

Figure 2 shows the results of SEM, AFM and CLSM data readouts from the surface of an exposed crystal at different radiation powers after exposure to 1-100 pulses. An interesting feature is a black spot at the central region of CLSM images (at the low dose rate cases). It corresponds to a dip in the intensity distribution inside the XFEL beam. This fact is explained by the feature of focusing CRL optics when its elements have geometrical imperfection as discussed in detail in our recent work [22].

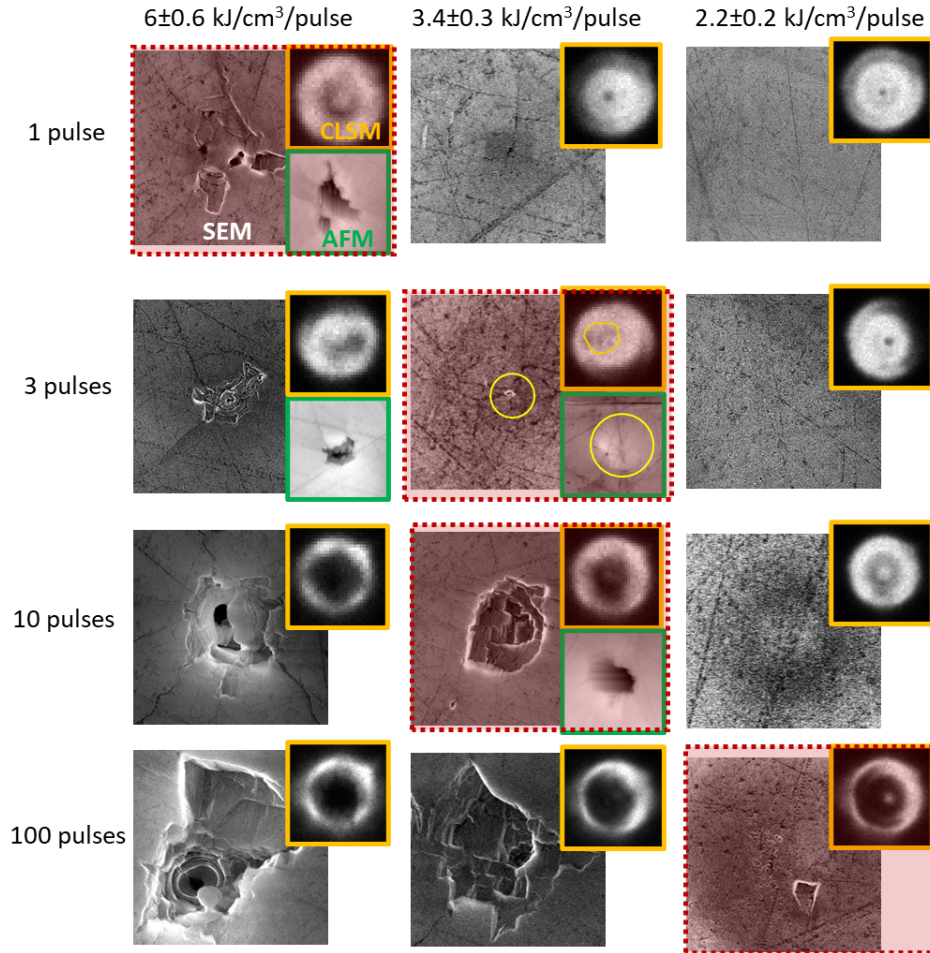


**Fig. 2.** – The results of measurements with different readout systems of the LiF crystal surface after irradiation with 1, 3, 10 and 100 pulses with dose rates of 2.2 – 6.0 kJ/cm<sup>3</sup>/pulse: large images, SEM; orange outlines, CLSM; green outlines, AFM. For all images, the field of view is 6 × 6 μm<sup>2</sup>. The images where damage begins for each irradiation mode are highlighted with wine-red frames.

As can be seen, the dose rate  $D_{rate}$  of 6.0 kJ/cm<sup>3</sup>/pulse of coherent femtosecond X-rays leads to crystal damage at all irradiation modes (1-100 pulses). When the  $D_{rate}$  is reduced to 3.4 kJ/cm<sup>3</sup>/pulse, no more surface ablation is observed for single-pulse irradiation, while swelling of the crystal surface occurs at 3 pulses (the area is outlined in yellow), which clearly represents

a threshold value. When irradiating with a sequence of ten X-ray pulses, the  $D_{rate}$  threshold at which crystal damage occurs is in the range of  $2.2 \text{ kJ/cm}^3/\text{pulse}$  -  $3.4 \text{ kJ/cm}^3/\text{pulse}$ . If the number of pulses  $N_{pulses}$  was increased to 100, ablation already starts to manifest at the  $D_{rate}$  of  $2.2 \text{ kJ/cm}^3/\text{pulse}$ . So, one can see a clear decrease in the damage threshold with an increase in the number of X-ray pulses.

Damage distribution caused by the hard X-ray pulses depends on the net dose absorbed in the material. At the relatively low dose rates in the range between the thresholds for brittle damage  $D_{rate}(brittle)$  and ablation  $D_{rate}(abl)$ , the damages of surface layer are observed in the form of cracks and ruptures, but ablation of the material with formation of crater does not occur. Such damage is typical of brittle materials, like lithium fluoride, but is unusual for the most metals. The ablation of surface material around the beam spot is caused by the higher dose rates above the ablation threshold  $D_{rate}(abl)$ , which leads to formation of a crater with a linear size larger than the beam diameter, and the surface cracks in a wide field surrounding the crater. For even higher dose rate beyond the threshold of deep damage,  $D_{rate}(cyl)$  a cylindrical-like cavity is formed in the material along the beam path, in addition to the cracks and crater [25].

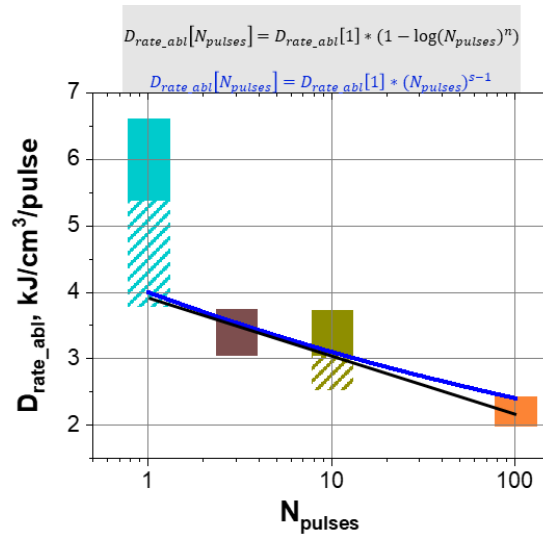
Thus, the area of brittle damage increases with increasing  $D_{rate}$  while the beam diameter remains almost constant. It indicates that the stress waves generated by the fast energy deposition within the relatively small beam diameter are responsible for formation of both the cracks and crater. It worth noting that the ablation of LiF is caused by its spallation, as seen in the AFM and SEM images presented in Fig. 2. It means that heating of material by an X-ray pulse is negligible outside the beam diameter, and the generated tensile stress waves exceed the local tensile strength of LiF in the crater area. The generation of such high-pressure waves is feasible because the heating is much shorter than the expansion time of heated material, which is provided by the shorter duration of X-ray pulse ( $\sim 20 \text{ fs}$ ) than the acoustic time ( $t_s = \text{FWHM}_{beam}/2c_s \sim 1 \text{ ps}$ ).

Figure 3 shows the damage thresholds in terms of  $D_{rate}$  found for each of the irradiation cases. The full fill marks the dose rate ranges where crystal ablation is clearly observed for each of the irradiation cases. The areas with broken shading correspond to the dose rates at which ablation could occur based on the data in Fig. 2, but we do not have accurate images in these areas. From the diagram in Fig. 3, we see that the ablation threshold decreases as the number of pulses incident on the crystal increases. Thus, the threshold dose is 2-3 times higher for single pulse irradiation than for 100 pulses. Note that the range of the  $D_{rate}$  threshold for the case of single pulse irradiation is near to the threshold of semiconductor (Si -  $5.75 \text{ kJ/cm}^3/\text{pulse}$ ) and metal (Pt -  $5.5 \text{ kJ/cm}^3/\text{pulse}$ ) occurs, which were found in the work [25] when irradiating with a SACLA XFEL femtosecond pulse with a photon energy of 10 keV. Finally, our experimental data was fitted by the following empirical formula:

$$D_{rate\_abl}[N_{pulses}] = D_{rate\_abl}[1pulse] * (1 - \log(N_{pulses})^n), \quad (1)$$

where  $D_{rate\_abl}[1 \text{ pulse}]$  — ablation threshold for single pulse irradiation (the value depends on the material) and  $n$  is a constant that takes into account the non-linear dependence of the threshold on the number of pulses.

Using the expression (1), the parameters of the approximation function were found:  $D_{rate\_abl}[1] = 3.9 \pm 0.27 \text{ kJ/cm}^3/\text{pulse}$  and  $n = 0.86 \pm 0.17$ , plotted in Fig. 3. Thus, we can conclude that the ablation threshold of LiF decreases for a pre-exposed crystal. In our case, we are dealing with a fluorescent dielectric in whose crystal lattice color centers accumulate from pulse to pulse. The accumulation of the dose means an increase in the concentration of F-type CCs, which weakens the binding energies between the atoms in the lattice and thus “loosens up” the substance. In the theoretical work [26], the influence of the concentration of color centers on the ablation threshold of LiF under soft X-ray pulses was investigated. In particular, it was found that defects can lower the ablation threshold several times due to the lattice destabilization and the tensile pressure caused by the defects when they are formed. The concentration of the F-type



**Fig. 3.** – The value of the ablation threshold, expressed in values of the  $D_{rate\_abl}$ , depends on the number of pulses irradiating the LiF crystal. The fitting parameters for the data are:  $D_{rate\_abl}[1] = 3.9 \pm 0.27$  kJ/cm<sup>3</sup>/pulse and  $n = 0.23 \pm 0.04$  for black line and  $D_{rate\_abl}[1] = 4 \pm 0.25$  kJ/cm<sup>3</sup>/pulse and  $s = 0.89 \pm 0.05$  for blue curve.

CCs  $f(D, D_{rate})$  as a function of the radiation dose  $D$  and the dose rate  $D_{rate}$  can be estimated using the empirical formula [24]:

$$f(D, D_{rate}) = k\sqrt{D} \left[ 1 + \log \left( 1 + \frac{D_{rate}}{D_{rate\_th}} \right)^2 \right], \quad (2)$$

where  $D_{rate\_th} = 10$  mJ cm<sup>-3</sup>s<sup>-1</sup> — threshold dose rate for LiF, above which nonlinear effects begin to appear during CCs generation;  $k = 8 \times 10^{15}$  J<sup>-1/2</sup> cm<sup>-3/2</sup> — coefficient constant for the LiF.

The concentration values of single CCs of F-type  $n_{F-centers}$ , calculated using Eq. (2), excited in a LiF crystal after irradiation with 1-100 pulses with the  $D_{rate} = 2.2$  kJ/cm<sup>3</sup>/pulse, are shown in Table 1. Taking into account that the concentration of lattice atoms of the LiF crystal is  $n_{LiF-atoms} \sim 6 \times 10^{22}$  cm<sup>-3</sup>, it can be seen that when the concentration of F-type CCs is increased by an order of magnitude (up to several percent of the total number of lattice atoms), the ablation threshold decreases by  $\sim 2.7$  times for irradiation with 100 pulses compared to single pulse irradiation. We can therefore assume that the threshold value does not drop significantly (logarithmic dependence) with irradiation with more than 100 pulses.

**Table 1.** Estimated values of the F-type CCs concentration  $n_{F-centers}$  activated in a LiF crystal upon irradiation with pulses with a constant dose rate  $D_{rate} = 2.2$  kJ/cm<sup>3</sup>/pulse. The values indicated in italics correspond to the case with the manifestation of ablation according to Fig. 2

N	$D_{rate}$ , kJ/cm <sup>3</sup> /pulse	$n_{F-centers}$ , cm <sup>-3</sup>	$n_{F-centers} / n_{LiF-atoms}$
1 pulse	2.2	$1.6 \times 10^{20}$	0.26%
3 pulses	2.2	$2.7 \times 10^{20}$	0.45%
10 pulses	2.2	$5.0 \times 10^{20}$	0.83%
100 pulses	2.2	$1.6 \times 10^{21}$	2.6%

On the other hand, the obtained reduction in threshold can be explained in terms of the incubation model [27]. This model was also used to explain the decrease in the ablation threshold of PMMA under soft X-ray pulses ( $\lambda = 27.2\text{--}34.3\text{ nm}$ ) [28] as well as for copper, silicon and gelatin under optical irradiation ( $\lambda = 800\text{ nm}$ ) [29]. The relation between single-shot threshold dose  $D_{\text{rate\_abl}}[1]$  and N-pulses threshold dose  $D_{\text{rate\_abl}}[N_{\text{pulses}}]$  has been proposed as given by:

$$D_{\text{rate\_abl}}[N_{\text{pulses}}] = D_{\text{rate\_abl}}[1\text{pulse}] * N_{\text{pulses}}^{S-1} \quad (3)$$

where  $S$  is called the incubation coefficient characteristic to the accumulation behavior (if  $S = 1$  implies no incubation effect).

Using the expression (3), the parameters  $D_{\text{rate\_abl}}[1] = 4.0 \pm 0.25\text{ kJ/cm}^3/\text{pulse}$  and  $S = 0.89 \pm 0.05$  were found. As can be seen in Fig. 3, the approximation curves constructed with Eqs. (1) and (3) are very close to each other (see black and blue curves plotted in Figure 3). We believe that the breaking of the lattice bond is one of the main reasons for lowering the threshold for LiF crystal. For soft matter, e.g. PMMA, the EUV laser pulse cause the chemical bond to break even with low fluence irradiation [28], and the accumulation of the laser pulse would also increase the deterioration of the chemical bond, like for case with the formation of color centers in LiF crystal.

### 3.2. Failure model for lithium fluoride

The results of the SEM measurements on the surface of lithium fluoride LiF show that the destruction of the material by a femtosecond pulse of the XFEL occurs when a certain threshold value of the energy input is exceeded. In a number of papers, there is also evidence that LiF samples are destroyed under dynamic or static loads by the formation of shear bands in which stress relaxation occurs [30,31]. In this case, the character of the destruction is similar to that observed in ceramic materials under high impact loading. In this context, we used a modified Johnson-Holmquist-Bessel failure model JHB [32–34] for ceramic materials with some modifications, which have been discussed in our previous works [35,36] to analyze a short pulsed impact on a LiF sample.

The basic idea of the JHB model is that the intact material (model damage parameter  $\mathcal{D} = 0$ ) has the strength limit  $\sigma_i(P)$  below which the only elastic loading is possible, Fig. 4(a). When this limit is reached, the failure process begins, which is characterized by a gradual loss of the shear strength. Such strength collapse is limited by  $\sigma_f < \sigma_i$ , which corresponds to the strength of the material in a completely failed state in the proposed model, Fig. 4(a). In this case, the damage kinetics is described by the following expression:

$$\frac{d\mathcal{D}}{dt} = (1 - \mathcal{D}) \frac{1}{\varepsilon_p^f} \frac{d\varepsilon_p}{dt}, \quad (4)$$

where  $d\varepsilon_p$  is an infinitesimal plastic strain increment at the time integration step  $dt$ ,  $\varepsilon_p^f$  is the total plastic strain of the completely failed state.

Compared to the original model [32–34], its modification, which is discussed in details in our previous work [35], adds the factor  $(1 - \mathcal{D})$  to expression (4). This dependence limits the value of  $\mathcal{D}$  from above to 1 and results in a smooth slowing down of the damage in the initial stages, whereas in the original model an acceleration of decay occurs. The total value of plastic deformations in a completely failed state in the context of the considered model is determined according to the definition of the increment of plastic deformations  $d\varepsilon_p$  as follows:

$$\varepsilon_p^f(P) = \frac{\sigma_i(P) - \sigma_f(P)}{3G}, \quad (5)$$

where  $G$  is the shear modulus of the material.

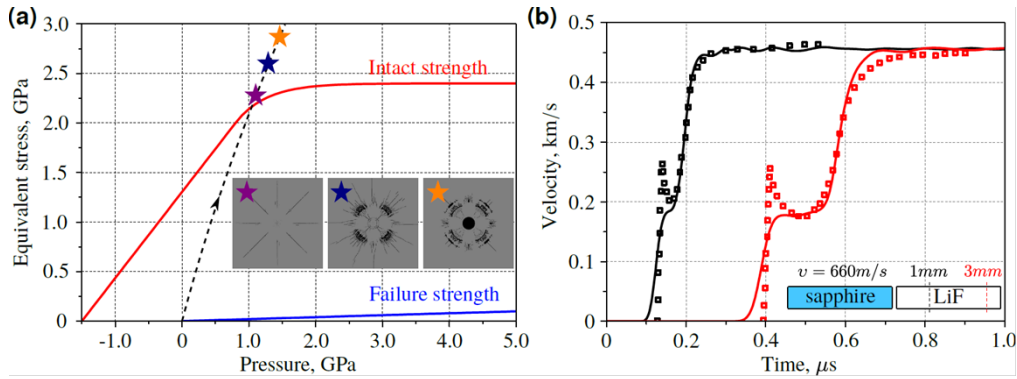


**Fig. 4.** – (a) Model strength curve of LiF in intact (red curve) and completely failed state (blue curve). The black dashed line corresponds to the elastic load of the material. The diagram contains images (top view) of the damage pattern at different energy inputs: 3.4 kJ/cm<sup>3</sup> (purple asterisks), 3.9 kJ/cm<sup>3</sup> (blue asterisks), 5.1 kJ/cm<sup>3</sup> (orange asterisks). Different asterisks on the plot show the feasible stresses, which can be obtained in the lithium fluoride without the usage of damage model. Grayscale corresponds to the degree of damage (black  $D = 1$ ) (b) Material velocity profiles inside the LiF sample at a depth of 0.98 mm (black markers and curve) and 2.98 mm (red markers and curve) from the collision site. The experimental data [31] are indicated with markers, the solid lines correspond to the simulation results.

A detailed description of the JHB model used and a step-by-step algorithm for its implementation can be found in work [35]. The mechanical properties and parameters for equation of state of the LiF are given in Table 2 [37,38].

**Table 2. Mechanical properties of lithium fluoride (LiF) and sapphire (Al<sub>2</sub>O<sub>3</sub>)**

Mechanical properties	LiF	Al <sub>2</sub> O <sub>3</sub>
Density $\rho_0$ , kg/m <sup>3</sup>	2650	3989
Shear modulus $G$ , GPa	55	151
Spall strength $\sigma_{sp}$ , GPa	1.5 (model)	10 [39]
Intact strength $\sigma_i$	2.4	-
Volumetric speed of sound $c_0$ , km/s	5.15	7.27
Shock coefficient $s_a$	1.35	1.533
Grüneisen parameter $\gamma$	0.71 [40]	1.5

To calibrate the constants of the failure model, shock wave experiments [31] were used in which the mass flow velocity produced by shocks propagating in the  $\langle 111 \rangle$  directions in single-crystal samples was recorded with electromagnetic velocity gauges. The simulations were performed using the meshless contact smoothed particles hydrodynamics method SPH [41,42]. On the graph in Fig. 4(b), the experimental velocity profiles are shown at a depth of 0.98 mm (black markers) and 2.98 mm (red markers) from the impact point of the LiF target with a sapphire impactor; the impactor velocity was 660 m/s. The simulation results are shown in the graph in Fig. 4(b) with curves in the corresponding color. It can be seen from the graph that the impact load in the experiments exceeds the damage limit of the material: The formation of an elastic precursor is observed, which propagates in the material at the longitudinal speed of sound, followed by the damage wave front. Note that stress relaxation occurs as a consequence of the damage to the LiF sample: as can be seen from the diagram in Fig. 4(b), the amplitude of the elastic precursor

first reaches its maximum value, after which its amplitude decreases significantly. The nature of the relaxation processes that determine this type of elastic wave profile in LiF is not known with certainty. It should also be noted that the failure model used does not reproduce the shape of the elastic precursor observed in experiments. However, its amplitude agrees well with the experimentally determined value, which indicates that the model should reliably reproduce the damage threshold of the material. Otherwise, it can be concluded from the comparison in the graph in Fig. 4(b) that a good agreement between the simulated and experimental velocity profiles was achieved.

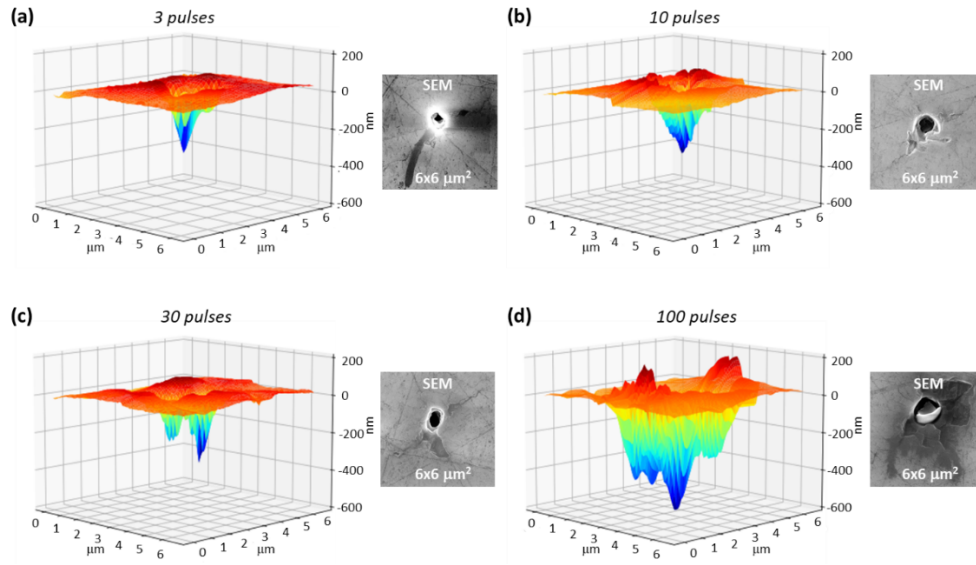
The calibrated LiF failure model was used to analyze the results of the SEM measurements of LiF. As in the shock-wave experiments [31], the single crystals are used in our study, but their orientations were not determined. In simulations, a 3D sample  $x \times y \times z = 10 \times 20 \times 20 \mu\text{m}^3$  ( $10 \mu\text{m}$  is into the depth of the sample) exposed to a femtosecond XFEL pulse is modelled by specifying an energy source within a cylindrical volume. The energy within this cylinder has a gaussian distribution with  $\text{FWHM} = 1 \mu\text{m}$  in the  $x \times y$  directions. According to work [40] the Grüneisen coefficient  $\gamma$  strongly decreases with temperature and is equal to 0.71 near the melting point. Such a value listed in Table 2 is used in our simulation to provide the calculated damage threshold  $\sim 3.4 \text{ kJ/cm}^3$  to be closed to the experimental one  $\sim 3.9 \text{ kJ/cm}^3$ . Depending on the energy deposited in the sample, a generated pressure pulse may exceed the energy density threshold for material failure. For higher energy density the failure bands are formed and propagate beyond the energy deposition region, similar to that observed in experiments. The damage pattern corresponding to such an energy deposition is shown in the inset marked with a purple star in Fig. 4(a). With increasing energy density, the damage area increases and form a “halo” around the cylindrical area where the energy is deposited, see the inset marked with a blue star in Fig. 4(a). The degree of damage grows up with further increasing of energy, but the area of damaged material increases only marginally, because the amplitude of diverging cylindrical shock wave decreases rapidly and soon it becomes below the damage threshold.

### 3.3. Crater morphology

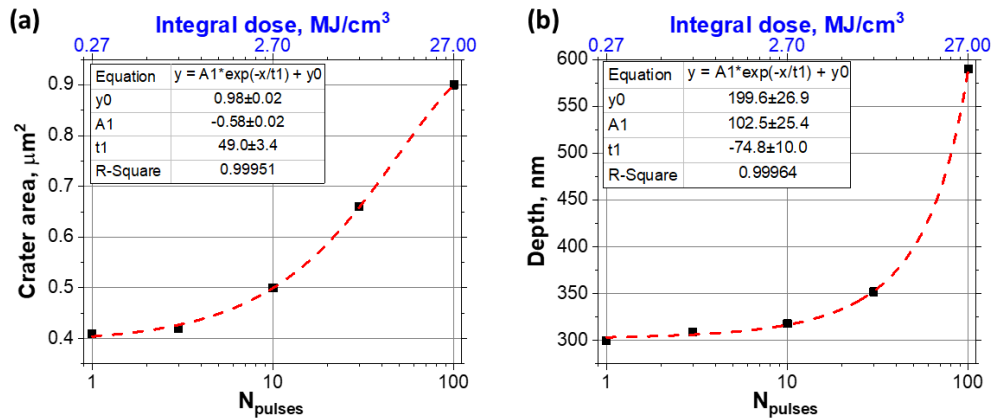
In the next step, we studied the morphology of the formed craters for the case of a maximum  $D_{\text{rate}}$  of  $270 \text{ kJ/cm}^3/\text{pulse}$  realized at the point of best focus of the X-ray beam ( $\text{FWHM} = 410 \text{ nm}$ ). The profile of the intensity distribution within the beam and its size were the same for exposures in the range of 1-100 pulses. Figure 5 shows the results of the AFM measurements for irradiation with 3, 10, 30 and 100 pulses. It can be seen that for irradiation with 3 pulses, a crater with a depth of  $\sim 310 \text{ nm}$  is formed, and the crystal surface is flat all around. As the number of pulses hitting the crystal increases, the depth and area of the crater increase, while nanostructures up to  $200 \text{ nm}$  high form on the surface around the crater, Fig. 5(b-d).

Figure 6 shows the dependence of the crater area and depth on the number of pulses incident on the LiF crystal. From general considerations, it seems that the dependence should be linear since the pulse duration is  $\sim 20 \text{ fs}$  and the repetition rate is  $\sim 100 \text{ ms}$ . Therefore, each subsequent pulse must interact with the already “cold” solid. However, as seen in Fig. 6(b), the depth of the crater depends non-linearly on the accumulated number of pulses (at a constant  $D_{\text{rate}}$ ).

It is interesting to compare the crater depths obtained in our work when irradiated with hard femtosecond X-ray pulses with similar measurements for the soft X-ray range. In work [17], when the ablation threshold was reached by picosecond pulses ( $\sim 7 \text{ ps}$ ) of a soft X-ray laser ( $E_{\text{ph}} = 89 \text{ eV}$ ), a crater with a depth of  $d \sim 30\text{--}55 \text{ nm}$  was formed on the surface of the LiF crystal, which is close to the attenuation length  $d_{\text{att}}[89 \text{ eV}] = 30 \text{ nm}$  for a given photon energy. The results of our AFM measurements, shown in Fig. 6(b), indicate that the depth of the formed craters is  $\sim 1000$  times smaller than the decay length  $d_{\text{att}}[9 \text{ keV}] = 475 \mu\text{m}$  for the photon energy  $E_{\text{ph}} = 9 \text{ keV}$ . We assume that the reason for the shallow depth of the crater is that the ablated LiF crystal in the region below the crater floor cannot be ejected outwards, which probably leads to a



**Fig. 5.** – AFM data for LiF crystal irradiation regime with constant  $D_{rate} = 270 \text{ kJ/cm}^3/\text{pulse}$ : (a) 3 pulses, (b) 10 pulses, (c) 30 pulses, (d) 100 pulses. For clarity, the data from SEM for each case are shown on the right.



**Fig. 6.** – Dependence of the area (a) and depth (b) of a formed crater in a LiF crystal as a function of the number of pulses incident on the surface. All data were obtained for one  $D_{rate} = 270 \text{ kJ/cm}^3/\text{pulse}$ , the results of AFM measurements of which are shown in Fig. 5.

solidification of the material and its amorphization. A similar effect was observed in work [25] when silicon was irradiated with XFEL pulses with a photon energy of 10 keV. It was showed the formation of a plug of a substance that clogged a long channel inside the sample. Within the scope of our work, we did not investigate this effect, which could be the subject of a separate article with additional measurements. For our AFM measurements, dynamic range (maximum value) of vertical depth was 2400 nm. However, since the beam diameter was too small in our experiment (FWHM = 410 nm) and damage around the formed crater had some nanostructures above the crystal surface, the tip of AFM cantilever could not reach the bottom of deep holes (width becomes larger as closer to the cantilever base). Thus, our measurements of crater depth

are a lower bound, but the trend of a non-linear dependence on the number of pulses is clearly visible.

### 3.4. Comparison of damage threshold between present results and soft x-ray/optical laser data

As mentioned in the introduction, the LiF crystal is often used as a fluorescent X-ray detector. In work [14], it was shown that when LiF is irradiated with a soft synchrotron source in accumulation mode (500 eV, dose rate 30 J/cm<sup>3</sup>/pulse), no ablation occurs at an accumulated dose up to 170 kJ/cm<sup>3</sup> and the sensitivity of the detector is ~20 mJ/cm<sup>3</sup>. Thus, the dynamic range of such a detector can reach a value of 10<sup>7</sup>. However, the damage of the crystal during irradiation with powerful ultrashort XFEL pulses reduces the dynamic range. Based on the values we determined for the thresholds for the ablation of the LiF crystal, the dynamic range decreases to ~ 1 × 10<sup>5</sup> - 2 × 10<sup>5</sup> when irradiated with femtosecond X-ray pulses with a dose rate of 2-4 kJ/cm<sup>3</sup>/pulse.

Let's now compare the values of the ablation thresholds determined in our work with earlier measurements from the literature. Figure 7 compares the ablation thresholds in terms of fluence and dose rate for different laser sources with the data obtained in our work. It can be seen that the fluence at which crystal ablation occurs is strongly dependent on the photon energy and pulse duration. From the data of a Ti:Sa laser (1.2 eV, "Optics" region in Fig. 7(a)) and X-ray lasers (26 eV and 89 eV, vacuum ultra-violet "VUV" region in Fig. 7(a)), it can be seen that the shorter the pulse incident on the crystal, the lower the threshold fluence [16] for the manifestation of LiF ablation at a constant photon energy. The values obtained in our work are more than 4 orders of magnitude higher than those found for an X-ray plasma laser with a pulse duration of 7 ps (Fig. 7(a)). However, moving to the consideration of the ablation threshold in units of dose rate, we find that the data agree well within the error limits with the measurements for a plasma laser with a picosecond pulse duration, Fig. 7(b). This fact suggests that for ultrashort pulses spanning the ps-fs range, ablation under the action of X-ray photons is achieved at a value of absorbed energy density of substance. Thus, for photons with energies in the range  $\gtrsim 100$  eV - 9 keV for ultrashort pulses (ps-, fs-), the ablation threshold is in the range 2-4 kJ/cm<sup>3</sup>/pulse. This fact can be explained by that the absorbed energy density provides a pressure required for generation of tensile stresses exceeding the spall strength  $\sigma_{sp}$  of material, which leads to ablation.

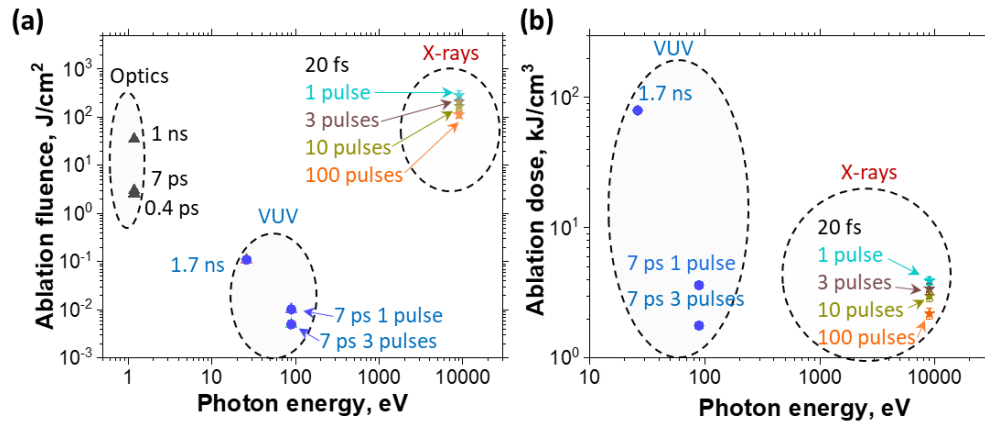


**Fig. 7.** - Threshold ablation laser fluence (a) and ablation dose (b) for the manifestation of damage in a LiF crystal as a function of laser source and photon energy. The ablation threshold for different pulsed laser systems is marked with a separate color. The data for the optical and VUV range were taken from [16,17,19,21] for comparison with the results obtained in this work – the X-ray range.

For ultrashort X-ray pulses,  $\sigma_{sp}$  is a constant and does not depend on the photon energy and attenuation length – it is only determined by the deformation rate in the tensile wave. Thus, to compare the ablation thresholds produced by different X-ray sources with ultrashort pulses the dose rate must be used instead of fluence as illustrated in Fig. 7.

#### 4. Conclusion

We investigated the multi-pulse damage threshold on LiF crystal under number of pulses in range 1-100. Combining the results obtained in our work with the available data for irradiation of a LiF crystal with coherent laser radiation in the soft X-ray/VUV range and for optical laser pulses, it was possible to show the dependencies of the ablation thresholds in a wide range of parameters – the energies of the incident photons, the pulse duration, and the accumulated dose. It was found that the ablation threshold of LiF crystal is determined only by the dose rate and does not depend on the photon energy  $E_{ph}$  for the ultrashort pulses in ps-fs range. We associate this fact with independence the spall strength  $\sigma_{sp}$  of material from these parameters. Also, an appreciable decrease in the ablation threshold was found in the case of multi-pulse irradiation. We associate this reduction with the lattice destabilization and the tensile pressure the color centers induce upon.

Our results enable the development of methods and possible technological approaches for the controlled nanomodification of the surface of dielectrics and, in particular LiF, using ultrashort coherent pulsed X-rays. Also, the presented data on the surface and depth morphology of the destruction of a lithium fluorine crystal can be used to verify numerical codes and models of the failure of dielectrics under the action of ultrashort X-ray pulses.

**Funding.** Ministry of Science and Higher Education of the Russian Federation (075-15-2021-1352); Japan Society for the Promotion of Science (21K03499); Grantová Agentura České Republiky (20-08452S).

**Acknowledgments.** The experimental results presented in this paper were obtained in December 2021. We greatly thank Alexander Pelka, Hauke Höppner, Carsten Baecht, Cornelius Strohm, Christian David, Clemens Prescher, Seniutinas Gediminas, Patrik Vagovic, Sebastian Göde and Andreas Schropp for their valuable contribution and support during the experiment. We acknowledge European XFEL in Schenefeld, Germany, for provision of X-ray free-electron laser beam time at HED SASE2 and would like to thank the staff for their assistance. We also thank Dr. Francesco Flora for useful discussions about LiF crystal readout procedure.

**Disclosures.** The authors declare no conflicts of interest.

**Data availability.** Data underlying the results presented in this paper are not publicly available at this time but may be obtained from the authors upon reasonable request.

#### References

1. K. Y. Yang, S. H. Hong, D. kee Kim, B. ki Cheong, and H. Lee, "Patterning of Ge<sub>2</sub>Sb<sub>2</sub>Te<sub>5</sub> phase change material using UV nano-imprint lithography," *Microelectron. Eng.* **84**(1), 21–24 (2007).
2. A. Kiani, K. Venkatakrishnan, B. Tan, and V. Venkataramanan, "Maskless lithography using silicon oxide etch-stop layer induced by megahertz repetition femtosecond laser pulses," *Opt. Express* **19**(11), 10834 (2011).
3. C. Shan, C. Zhang, J. Liang, Q. Yang, H. Bian, J. Yong, X. Hou, and F. Chen, "Femtosecond laser hybrid fabrication of a 3D microfluidic chip for PCR application," *Opt. Express* **28**(18), 25716 (2020).
4. A. Vetter, R. Kirner, D. Opalevs, M. Scholz, P. Leisching, T. Scharf, W. Noell, C. Rockstuhl, and R. Voelkel, "Printing sub-micron structures using Talbot mask-aligner lithography with a 193 nm CW laser light source," *Opt. Express* **26**(17), 22218 (2018).
5. D. V. Bochek, K. B. Samusev, D. A. Yavsin, M. V. Zhukov, M. F. Limonov, M. V. Rybin, I. I. Shishkin, and A. D. Sinelnik, "Fabrication of Ge<sub>2</sub>Sb<sub>2</sub>Te<sub>5</sub> metasurfaces by direct laser writing technique," *Opt. Laser Technol.* **141**(February), 107124 (2021).
6. T. Lee, C. Lee, D. K. Oh, T. Badloe, J. G. Ok, and J. Rho, "Scalable and high-throughput top-down manufacturing of optical metasurfaces," *Sensors* **20**(15), 4108 (2020).
7. G. V. Odintsova, E. A. Vlasova, Y. M. Andreeva, M. K. Moskvina, A. S. Krivososov, E. V. Gorbunova, D. V. Pankin, O. S. Medvedev, M. M. Sergeev, N. N. Shchedrina, D. S. Lutoshina, and V. P. Veiko, "High-resolution large-scale plasmonic laser color printing for jewelry applications," *Opt. Express* **27**(3), 3672 (2019).
8. E. Sharma, R. Rath, J. Misharwal, B. Sinhar, S. Kumari, J. Dalal, and A. Kumar, "Evolution in Lithography Techniques: Microlithography to Nanolithography," *Nanomaterials* **12**(16), 2754 (2022).
9. L. V. Keldysh, "Ionization in the field of a strong electromagnetic wave," *Sov. Phys. JETP* **20**(5), 1307–1314 (1965).

10. B. Rethfeld, "Unified model for the free-electron avalanche in laser-irradiated dielectrics," *Phys. Rev. Lett.* **92**(18), 187401 (2004).
11. I. Y. Skobelev, A. Y. Faenov, T. A. Pikuz, and V. E. Fortov, "Spectra of hollow ions in an ultradense laser plasma," *Phys.-Usp.* **55**(1), 47–71 (2012).
12. S. B. Hansen, J. Colgan, and A. Y. Faenov, *et al.*, "Detailed analysis of hollow ions spectra from dense matter pumped by X-ray emission of relativistic laser plasma," *Phys. Plasmas* **21**(3), 031213 (2014).
13. G. Rigon, B. Albertazzi, and T. Pikuz, *et al.*, "Micron-scale phenomena observed in a turbulent laser-produced plasma," *Nat. Commun.* **12**(1), 2679 (2021).
14. S. Makarov, S. Pikuz, S. Ryazantsev, T. Pikuz, A. Buzmakov, M. Rose, S. Lazarev, T. Senkbeil, A. Von Gundlach, S. Stuhr, C. Rumancev, D. Dzhigaev, P. Skopintsev, I. Zaluzhnyy, J. Viefhaus, A. Rosenhahn, R. Kodama, and I. A. Vartanyants, "Soft X-ray diffraction patterns measured by a LiF detector with sub-micrometre resolution and an ultimate dynamic range," *J. Synchrotron Radiat.* **27**(3), 625–632 (2020).
15. S. S. Makarov, I. A. Zhvania, S. A. Pikuz, T. A. Pikuz, and I. Y. Skobelev, "Study of the Parameters of a High-Intensity Thermal and Coherent X-ray Sources with the Use of LiF Crystal Detector (Review)," *High Temp.* **58**(4), 615–631 (2020).
16. B. Stuart, M. Feit, S. Herman, A. Rubenchik, B. Shore, and M. Perry, "Nanosecond-to-femtosecond laser-induced breakdown in dielectrics," *Phys. Rev. B* **53**(4), 1749–1761 (1996).
17. A. Y. Faenov, N. A. Inogamov, V. V. Zhakhovskii, V. A. Khokhlov, K. Nishihara, Y. Kato, M. Tanaka, T. A. Pikuz, M. Kishimoto, M. Ishino, M. Nishikino, T. Nakamura, Y. Fukuda, S. V. Bulanov, and T. Kawachi, "Low-threshold ablation of dielectrics irradiated by picosecond soft x-ray laser pulses," *Appl. Phys. Lett.* **94**(23), 2012–2015 (2009).
18. N. A. Inogamov, A. Y. Faenov, V. A. Khokhlov, V. V. Zhakhovskii, Y. V. Petrov, I. Y. Skobelev, K. Nishihara, Y. Kato, M. Tanaka, T. A. Pikuz, M. Kishimoto, M. Ishino, M. Nishikino, Y. Fukuda, S. V. Bulanov, T. Kawachi, S. I. Anisimov, and V. E. Fortov, "Spallative ablation of metals and dielectrics," *Contrib. Plasma Phys.* **49**(7–8), 455–466 (2009).
19. N. A. Inogamov, V. V. Zhakhovsky, and A. Y. Faenov, *et al.*, "Ablation of insulators under the action of short pulses of X-ray plasma lasers and free-electron lasers," *J. Opt. Technol.* **78**(8), 473 (2011).
20. N. A. Inogamov, S. I. Anisimov, and V. V. Zhakhovsky, *et al.*, "Ablation by short optical and x-ray laser pulses," in *Proc. of SPIE*, V. P. Veiko and T. A. Vartanyan, eds. (2011), 7996, p. 79960T.
21. T. Blejchar, V. Nevrlý, M. Vašínek, M. Dostál, M. Kozubková, J. Dlabka, M. Stachon, L. Juha, P. Bitala, Z. Zelinger, P. Pira, and J. Wild, "Desorption/ablation of lithium fluoride induced by extreme ultraviolet laser radiation," *Nukleonika* **61**(2), 131–138 (2016).
22. S. Makarov, M. Makita, and M. Nakatsutsumi, *et al.*, "Direct LiF imaging diagnostics on refractive X-ray focusing at the EuXFEL High Energy Density instrument," *J. Synchrotron Radiat.* **30**(1), 208–216 (2023).
23. "X-Ray Database," <https://henke.lbl.gov/>.
24. G. Baldacchini, S. Bollanti, and F. Bonfigli, *et al.*, "Soft x-ray submicron imaging detector based on point defects in LiF," *Rev. Sci. Instrum.* **76**(11), 1–12 (2005).
25. T. Koyama, H. Yumoto, Y. Senba, K. Tono, T. Sato, T. Togashi, Y. Inubushi, T. Katayama, J. Kim, S. Matsuyama, H. Mimura, M. Yabashi, K. Yamauchi, H. Ohashi, and T. Ishikawa, "Investigation of ablation thresholds of optical materials using 1- $\mu$ m-focusing beam at hard X-ray free electron laser," *Opt. Express* **21**(13), 15382 (2013).
26. Y. Cherednikov, N. A. Inogamov, and H. M. Urbassek, "Influence of defects on extreme ultraviolet laser ablation of LiF," *Phys. Rev. B* **88**(13), 134109 (2013).
27. Y. Jee, M. F. Becker, and R. M. Walser, "Laser-induced damage on single-crystal metal surfaces," *J. Opt. Soc. Am. B* **5**(3), 648 (1988).
28. K. Sakaue, H. Motoyama, R. Hayashi, A. Iwasaki, H. Mimura, K. Yamanouchi, T. Shibuya, M. Ishino, T.-H. Dinh, H. Ogawa, T. Higashiguchi, M. Nishikino, and R. Kuroda, "Surface processing of PMMA and metal nano-particle resist by sub-micrometer focusing of coherent extreme ultraviolet high-order harmonics pulses," *Opt. Lett.* **45**(10), 2926 (2020).
29. C. S. R. Nathala, A. Ajami, W. Husinsky, B. Farooq, S. I. Kudryashov, A. Daskalova, I. Bliznakova, and A. Assion, "Ultrashort laser pulse ablation of copper, silicon and gelatin: effect of the pulse duration on the ablation thresholds and the incubation coefficients," *Appl. Phys. A* **122**(2), 107 (2016).
30. W. D. Scott and J. A. Pask, "Deformation and Fracture of Polycrystalline Lithium Fluoride," *J. Am. Ceram. Soc.* **46**(6), 284–293 (1963).
31. G. Rosenberg and G. E. Duvall, "Precursor amplitudes in LiF from shocks propagating in  $\langle 111 \rangle$  directions," *J. Appl. Phys.* **51**(1), 319–330 (1980).
32. G. R. Johnson and T. J. Holmquist, "Response of boron carbide subjected to large strains, high strain rates, and high pressures," *J. Appl. Phys.* **85**(12), 8060–8073 (1999).
33. G. R. Johnson, T. J. Holmquist, and S. R. Beissel, "Response of aluminum nitride (including a phase change) to large strains, high strain rates, and high pressures," *J. Appl. Phys.* **94**(3), 1639–1646 (2003).
34. T. J. Holmquist and G. R. Johnson, "Characterization and evaluation of silicon carbide for high-velocity impact," *J. Appl. Phys.* **97**(9), 093502 (2005).
35. S. A. Dyachkov, A. N. Parshikov, M. S. Egorova, S. Y. Grigoryev, V. V. Zhakhovsky, and S. A. Medin, "Explicit failure model for boron carbide ceramics under shock loading," *J. Appl. Phys.* **124**(8), 085902 (2018).

36. S. Y. Grigoryev, S. A. Dyachkov, A. N. Parshikov, and V. V. Zhakhovsky, "Failure model with phase transition for ceramics under shock loading," *J. Appl. Phys.* **131**(12), 125106 (2022).
37. T. Ao, M. D. Knudson, J. R. Asay, and J. P. Davis, "Strength of lithium fluoride under shockless compression to 114 GPa," *J. Appl. Phys.* **106**(10), 103507 (2009).
38. J.-P. Davis, M. D. Knudson, L. Shulenburg, and S. D. Crockett, "Mechanical and optical response of [100] lithium fluoride to multi-megabar dynamic pressures," *J. Appl. Phys.* **120**(16), 165901 (2016).
39. I. A. Cherepanov, A. S. Savinykh, and S. V. Razorenov, "Spalling in Sapphire in Different Crystallographic Directions under Shock Compression," *Tech. Phys.* **65**(6), 921–924 (2020).
40. P. D. Pathak and N. G. Vasavada, "Thermal expansion of LiF by X-ray diffraction and the temperature variation of its frequency spectrum," *Acta Crystallogr., Sect. A: Cryst. Phys., Diff., Theor. Gen. Crystallogr.* **28**(1), 30–33 (1972).
41. A. N. Parshikov and S. A. Medin, "Smoothed Particle Hydrodynamics Using Interparticle Contact Algorithms," *J. Comput. Phys.* **180**(1), 358–382 (2002).
42. M. S. Egorova, S. A. Dyachkov, A. N. Parshikov, and V. V. Zhakhovsky, "Parallel SPH modeling using dynamic domain decomposition and load balancing displacement of Voronoi subdomains," *Comput. Phys. Commun.* **234**, 112–125 (2019).